2014 IEEE Congress on Evolutionary Computation (CEC)
July 6-11, 2014, Beijing, China

Remote Sensing Imagery Clustering Using An Adaptive Bi-Objective Memetic Method

Ailong MA, Yanfei Zhong*, and Liangpei Zhang
The State Key Laboratory of Information Engineering in Surveying, Mapping and Remote Sensing (LIESMARS)
Wuhan Universtiy (WHU)
Wuhan, P.R.C
(* *corresponding author*) E-mail:{maailong007, zhongyanfei, zlp62}@whu.edu.cn

***Abstract*—Due to the intrinsic complexity of the remote sensing image and the lack of the prior knowledge, clustering for remote sensing image has always been one of the most challenging works in remote sensing image processing. The proposed algorithm constructs a bi-objective memetic-based framework, exploiting the feature space more efficiently. In the framework, two objective functions, Jm and XB, are used as the objective functions for bi-objective optimization. Furthermore, an adaptive local search method which can dynamically adjust its parameter value according to the selection probability has been developed and incorporated into the proposed algorithm. In order to speed the convergence and obtain more non-dominated solutions in the pareto front, a new strategy is newly devised in the local search process, which considers more solutions as the candidate for the next generation. To evaluate the proposed algorithm, some experiments on two multi-spectral images are conducted. The results show that the proposed algorithm can achieve better performance, compared with related methods.**

***Keywords*—memetic; multi-objective; remote sensing; fuzzy clustering**

I. INTRODUCTION

Clustering is one of the most important techniques in remote sensing image processing. The aim of remote sensing clustering is to partition a given image into groups such that pixels in the same group are as similar to each other as possible, while those assigned to different groups are dissimilar. Among the clustering methods, fuzzy clustering is popular and has been widely used in remote sensing image clustering. The fuzzy clustering approach can retain more information from the original image than the crisp or hard clustering methods such as K-means and ISODATA, which usually do not perform well when the mixed pixel problem appears.

In literature, the remote sensing image clustering was completed by minimizing or maximizing the corresponding objective function, which models the structure of the remote sensing image. However, different types of remote sensing images have different structures. It is unreasonable to use only one objective function for the clustering task because of the fact that no single clustering objective function works equally well for different kinds of remote sensing images, especially considering the complexity of remote sensing images. Thus, it is natural to simultaneously optimize multiple clustering objective functions for capturing different characteristics of the remote sensing images, which is usually named as multi-objective optimization [1]. Recently, some multi-objective evolutionary clustering algorithms for remote sensing image are available in the literature [2], [3], In [2], zhong *et. al* design a two-layer system comprising an optimization layer and classification layer. In the classification layer, NSGA-II [4] is utilized to minimize the Jm value and Xie-Beni index. In [3], Andrea Paoli *et al* present new methodology for clustering hyperspectral images within a multi-objective particle optimization framework, which can implement feature selection, determination of cluster number and clustering simultaneously. However, the traditional optimization methods such as differential evolution algorithm (DE) or simulated annealing, cannot capture the global search capability and local search capability simultaneously. For example, DE, as one of the stochastic search algorithms, has powerful global search capability [5]. Although DE can locate the promising solutions of the search space, it is difficult for them to refine the solutions in the space due to lack of local search capability, which can result in unsatisfactory remote sensing image clustering results.

In this paper, in order to resolve the above problem in remote sensing image clustering, an adaptive bi-objective memetic fuzzy clustering algorithm for remote sensing imagery (ABOMC) is proposed. Our contributions are as follows:

- A bi-objective memetic framework is used to cluster remote sensing image. In this framework, two objective functions Jm and XB are optimized by memetic algorithms (MAs) [6], which are computational framework based on the cultural evolution that can exhibit local refinement. MAs consist of global search and local search, which can combine the global search capability of evolution algorithm and individual refining of local search. In the proposed framework, differential evolution algorithm (DE) is used as the global search method because of its powerful global search capability [5]

This work was supported by the National Natural Science Foundation of China under Grant No. 41371344，A Foundation for the Author of National Excellent Doctoral Dissertation of P.R. China (FANEDD) under Grant No. 201052，Program for Changjiang Scholars and Innovative Research Team in University (IRT1278), and 863 High Technology Program of the People's Republic of China under Grant No. 2013AA12A301.

and it has also been used to many applications of remote sensing image processing [7]-[10]. Gaussian local search is used as the local search method. In MAs, a meme is often taken as a local search method. The selection of meme is essential to the performance of MAs. The bad meme cannot enhance the search capability but deteriorates its performance. Hence, the selection of meme is also important to remote sensing clustering result.

- In the bi-objective memetic framework, a strategy is used to resolve the above problem by determining the parameter in MAs, which can control the local search capability, resulting in much more satisfactory remote sensing clustering result.
- In the process of local search, a new strategy is proposed to speed up the convergence and obtain more non-dominated solutions in the process of local search.

The rest of the paper is organized as follows. Section II introduces some related background, including multi-objective optimization (MO), the objective function used in this paper, and memetic algorithms (MAs). Section III describes the proposed algorithm in detail. The experimental results are shown in Section IV, and Section V provides the conclusion.

II. Background

A. Multi-Objective Optimization

A multi-objective optimization problem can be generally defined to search the vector $x^* = [x_1^*, x_2^* \ldots x_n^*]^T$ of decision variables which satisfies the p equality constraints:

$$h_i(x) = 0; \quad i = 1, 2, ..., p; \tag{1}$$

the m inequality constraints:

$$g_i(x) \geq 0; \quad i = 1, 2, ..., m; \tag{2}$$

and optimizes the vector function:

$$g_i(x) \geq 0; \quad i = 1, 2, ..., m; \tag{3}$$

The constraints shown in (2) and (3) define the feasible region which contains all the admissible solutions. Any solution outside this region is inadmissible since it violates one or more constraints. To describe the multi-objective optimization problem, the following concepts need to be defined.

(1) If $\forall i \in [1, 2, ..., k] \quad f_i(x_1) \leq f_i(x_2), \quad \exists f_i(x_1) \neq f_i(x_2)$ x_1 dominates x_2 .

(2) The vector x^* denotes an optimal solution when no any other solution can dominate x^* . The set contains all optimal solutions is called Pareto Front.

In literature, different methods have been proposed to resolve the multi-objective optimization. In [11], in order to resolve the multi-objective optimization, a weight sum of the several normalized cluster validity functions is proposed. In [12], decomposition-based MOEA (MOEA/D) is proposed, which decomposed a multi-objective optimization problem into a number of scalar optimization subproblems and optimizes them simultaneously. In [13], Aimin Zhou et al survey the development of MOEAs primarily during recent years. It covers algorithmic frameworks such as decomposition-based MOEA (MOEA/D), memetic MOEAs, coevolutionary MOEAs, MOEAs for multimodal problems etc.

The most popular multi-objective optimization algorithm is the fast and elitist non-dominated sorting genetic algorithm for multi-objective optimization (NSGA-II), in which the crowding distance is introduced to increase the diversity of the population. The strategy of NSGA-II has got most experts' approval and is often the comparison method with the newly proposed multi-objective-based methods. In this paper, NSGA-II is also accepted as our multi-objective optimization framework.

In this paper, two objective functions are tested: XB and Jm, the formulas of which are (4) and (5).

$$Jm = \sum_{i=1}^{C} \sum_{k=1}^{N} u_{ik}^m \| x_k - v_i \|^2 \tag{4}$$

$$\mathrm{X}B = \frac{J_m / N}{Sep(v)} = \frac{\sum_{i=1}^{C} \sum_{k=1}^{N} u_{ik}^m \left\| x_k - v_i \right\|^2}{N \min_{i \neq j} \left\| v_i - v_j \right\|^2} \tag{5}$$

where x_k is the gray-level value of the *k*-th pixel as for the original remote sensing image; *N* is the total number of pixels; *C* is the number of clusters; v_i is the value of the *i*-th cluster center; and u_{ik} represents the fuzzy membership of the *k*-th pixel.

B. Memetci Algorithms (MAs)

The traditional clustering algorithms, such as K-means and FCM, belong, in essence, to mountain-climbing methods. That is, it is easy for them to get stuck in a local optimum. Some global optimization methods such as the genetic algorithm, differential evolution algorithm, and clonal selection algorithm have been used to optimize the corresponding objective functions. Although these global optimization methods can locate the promising solutions of the search space, it is difficult for them to refine the solutions in the space. Hence, the optimization performance is usually unsatisfactory if only one optimization method is utilized to optimize the objective function. Hence, a memetic algorithm is needed, which can be seen as a population-based search method that is coupled with one or more local search methods.

As can be seen from Fig. 1, the general framework of the memetic algorithm is the same as a traditional evolution algorithm such as the genetic algorithm or differential evolution algorithm, except for the addition of a local search procedure that refines some individuals of the population. The success of the memetic algorithm is therefore largely dependent on the selection of the local search method or its local search capability, which often incorporates domain knowledge of the specific problem. Recently, some memetic-based method has been proposed to tackle the problem [14], [15].

Input: an instance, size of population,

Output: a feasible individual

Initialization: Generate an initial population
While stopping criteria are not satisfied do
  Evaluate all individuals in the population
  Evolve a new population using evolutionary operator
    for each suitable individual
      Perform local search around it
    end
end

Fig. 1 General framework of the memetic algorithm

III. THE PROPOSED METHOD

In this paper, an adaptive bi-objective memetic fuzzy clustering algorithm for remote sensing imagery (ABOMC) is proposed.

A. ABOMC

In ABOMC, a bi-objective memetic framework is used for remote sensing image clustering. NSGA-II is accepted as the bi-objective optimization framework. Meanwhile, a variant of differential evolution, jDE [16], is set as the evolution algorithm in bi-objective optimization. The flowchart of ABOMC is as Fig. 3, which will be described in detail below.

Step 1. Initialization of the population.

In jDE, the mutation scale factor F and the crossover constant CR need to be encoded into individual. An example of individual encoding is shown in Fig. 2. In the process of initialization, the pixels are randomly selected from the whole image as the cluster centers in the corresponding individual.

9.8	15.6	8.2	17.3	7.5	14.6	0.8	0.3
Center 1		Center 2		Center 3		CRi	Fi

Fig. 2 An example of individual encoding

Step 2. Calculation of the objective function value of each individual, namely the corresponding clustering validity indices (4) and (5).

Step 3. Adaptive mutation and crossover.

In DE, the mutation operator amounts to creating a donor vector $\boldsymbol{V}_i(t)=[v_{i,1}(t),v_{i,2}(t),...,v_{i,D}(t)]$ for changing each individual of the population. The mutation process can be expressed as follows:

$$\boldsymbol{V}_i(t)=\boldsymbol{X}_{r_1^i}(t)+F_i(\boldsymbol{X}_{r_2^i}(t)-\boldsymbol{X}_{r_3^i}(t)) \tag{6}$$

where $\boldsymbol{X}_{r_1^i}(t),\boldsymbol{X}_{r_2^i}(t),\boldsymbol{X}_{r_3^i}(t)$ are picked up randomly from the population.

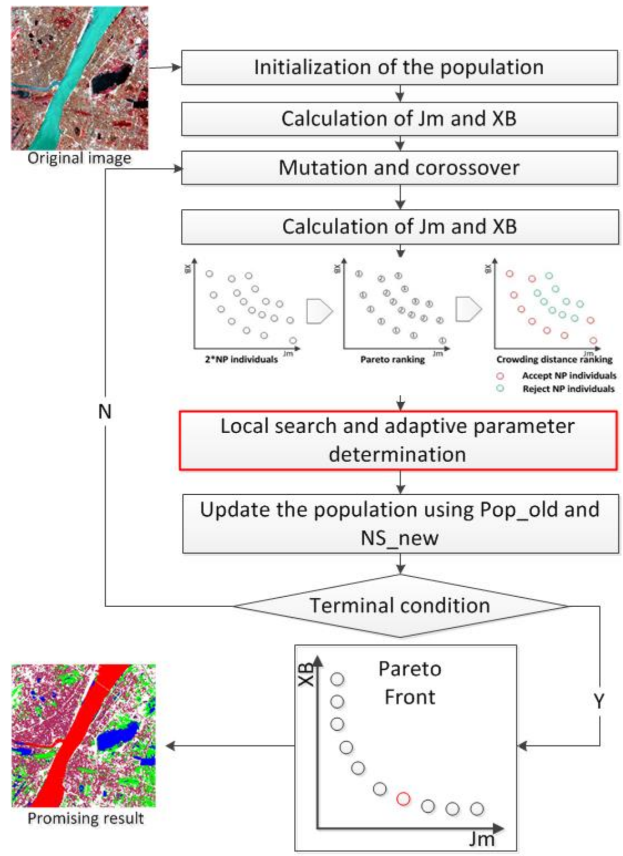

Fig. 3 The flowchart of ABOMC

After the mutation operator, crossover is undertaken between the donor vector $\boldsymbol{V}_i(t)$ and the target vector $\boldsymbol{X}_i(t)$, generating a trial vector $\boldsymbol{U}_i(t)=[u_{i,1}(t),u_{i,2}(t),...,u_{i,D}(t)]$. The crossover operator can be implemented as follows:

$$u_{i,j}(t)=\begin{cases} v_{i,j}(t), \text{ if } (\text{rand}_{i,j}(0,1)\le CR_i \text{ or } j=j_{rand}) \\ x_{i,j}(t), \textit{ otherwise} \end{cases} \tag{7}$$

There are two main parameters, F and CR, in DE. As is shown in Fig. 2, each individual not only encodes the cluster centers but also the parameters F and CR, enabling their update in the process of evolution. F_i and CR_i can be updated according to (8) and (9).

$$F_i^{'}=\begin{cases} 0.1+0.9\times rand(0,1), & if\ rand(0,1)<0.1 \\ F_i, & otherwise \end{cases} \tag{8}$$

$$CR_i^{'}=\begin{cases} rand(0,1), & if rand(0,1)\le 0.1 \\ CR_i, & otherwise \end{cases} \tag{9}$$

where $F_i^{'}$ and $CR_i^{'}$ are the updated values of the corresponding individual.

Step 4. Calculation of the objective function values of each individual by using (4) and (5).

Step 5. Non-dominated ranking

Among the population, different individuals are compared with the concept of pareto domination. If one individual are not dominated by all other individuals, then label its pareto front number with 0. All individuals with pareto front number 1 should be deleted temporally. Among the remaining individuals, different individuals are compared with the concept of pareto domination. If one individual are not dominated by all other individuals, then label its pareto front number with 2. Repeat the above population until all the individuals are labelled with its pareto front number.

Step 6. Crowding distance ranking

After the stochastic operation on the population, the size of the whole population becomes 2**NP*. Hence, *NP* individuals need to be selected to enter the next generation. However, the competition happens when the individuals are in the same non-dominated front. Crowding distance need to calculate in order to estimate the density of the solutions. The individuals with larger crowding distance will be selected to enter the next generation. The crowding distance can be calculated as below:

$$DIS_i = \frac{f_1(x_{i-1}) - f_1(x_{i+1})}{f_1^{\max} - f_1^{\min}} + \frac{f_2(x_{i+1}) - f_2(x_{i-1})}{f_2^{\max} - f_2^{\min}} \tag{10}$$

Where $f_1(.)$ and $f_2(.)$ are the objective functions (4) and (5). $f_1^{\max}, f_1^{\min}, f_2^{\max}, f_2^{\min}$ are the maximum and minimum value of different objective functions.The process of pareto ranking and crowding distance ranking is shown in Fig. 4.

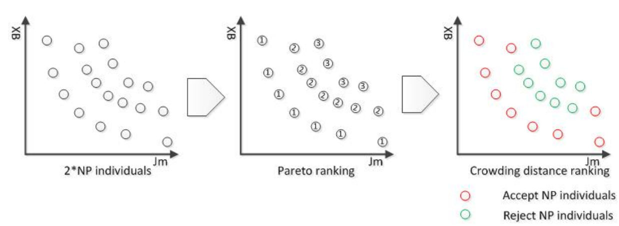

Fig. 4 Pareto ranking and crowding distance ranking

Step 7. After step 5 and step 6, *NP* individuals are selected to enter the new population. Then the local search is performed on the new population, which will be described in detail in the next part.

Step 8. In the process of local search, a population *NS_new* will be obtained. Then *NS_new* population and the refined population will be combined to generate a new larger population. In general, the size of the new larger population is larger than *NP*. The operations in step 5 and step 6 will be used to select *NP* individuals from the new larger population.

Step 9. Repeat step 3 to step 8 until the terminal condition can be fulfilled.

Step 10. The cluster in the pareto front will be used to cluster the remote sensing image.

B. Local Search- Gaussian Local search (GLS)

As for each individual in the population, a local search is performed on the individual j whenever a random number between 0-1 is larger than FLS. A Gaussian mutation is performed on each cluster of the individual. In this paper, FLS is 0.5, namely 50 percent of the individuals in the population need to local search.

Local search is an important part of the memetic algorithm. The role of the local search is fundamental, and the selection of its search rule and its balance with the global search scheme determine the success of the memetic framework. The local search method used in this paper is as follows.

Suppose that $x(k) = \{x_1(k), x_2(k), ..., x_N(k)\}$ is a vector with N dimensions that represents a cluster center. The Gaussian mutation can be represented as (11).

$$x_i'(k) = N(x_i(k-1), \delta^2) \tag{11}$$

Where $i \in [1, N]$, and $N(x_i(k-1), \delta^2)$ is a normal distribution with a mean of $x_i(k-1)$ and standard deviation δ .

The Gaussian mutation is performed on each dimension of the vector. As for the minimization problem, the individual with the best fitness obtained by the global search can be updated as follows.

Input: individual to local search

Output: better individual and non-dominated individuals in population NS_new

For each dimension in the individual

- Perform the Gaussian mutation to produce a trial individual.
- Evaluate the trial individual by (8) and (9).
- Pareto_Judge the trial individual and target individual.

end

Fig. 5 Gaussian local search

Fig. 5 shows the process of GLS. Trial individuals are generated by performing Gaussian mutation on the target individual. The operator Pareto_Judge will be performed between the trial solution and the target solution, which will be described in detail in the part C and Fig. 6.

As can be seen from (11), the parameter δ is crucial to the GLS. In this paper, a new strategy is applied to adaptively determine the parameter δ, which will be described in detail in part C.

C. Update Parameter of Local Search

In the process of evolution, many individuals are generated. However, the information encoded in them is not utilized fully. For example, the individual fitness increment between before and after local search can be gathered and used to determine the parameter δ in local search. The bigger the individual fitness increment is, the bigger the probability of the parameter δ value is. The whole process of updating parameter δ in local search is listed in Fig. 7. The strategy can be described as follows.

In order to simplify the parameter δ determination, there are only four parameter δ values, namely 0.01, 0.1, 1, 10. As for each value, the probability that they could be selected is stored in PLS. The initial value of PLS for each parameter δ is 0.25.

Step 1. As for each individual $individual_i$ that needs to local search, a roulette selection strategy is applied on PLS to select the parameter δ value j.

Step 2. $individual_{inew}$ is generated when Gaussian local search is applied on the $individual_i$. Then an operator named Pareto_Judge is performed between $individual_i$ and $individual_{inew}$. If $individual_{inew}$ dominates $individual_i$, $individual_{inew}$ substitutes $individual_i$ to enter the population. If they both don't dominate each other, then $individual_{inew}$ enter a new population named NS_new. An example is shown in Fig. 7. In the example it is assumed that it is a minimization problem. As for the individual (red) that needs to be local search, the individual (green) will substitute the individual (red) and the individual (blue) will enter the new population NS_new. The individual (yellow) will be rejected.

Step 3. When $individual_{inew}$ dominates $individual_i$, the individual fitness increment of jth parameter parameter δ can be calculated with (12), in order to score the jth parameter δ.

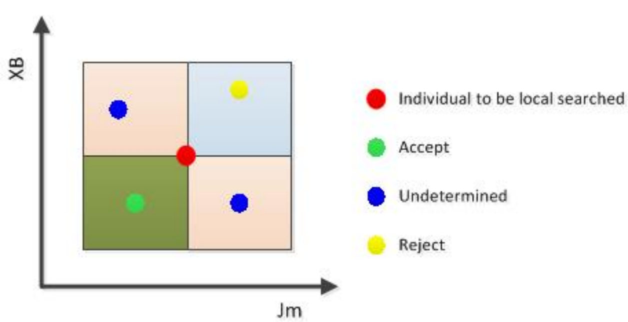

Fig. 6 Pareto_Judge strategy

$$\mathrm{Score}_j = \frac{f_1 - \hat{f}_1}{\hat{f}_1} + \frac{f_2 - \hat{f}_2}{\hat{f}_2} \tag{12}$$

Where f_1 and f_2 represent the values of Jm and XB before local search. $\hat{f}_1$ and $\hat{f}_2$ represent the values of Jm and XB after local search.

Step 4. AS_j is can be calculate by using (13). AS_j can be seen as the average score for the *j*-th parameter parameter δ. Num_j indicates the number of times that the *j*-th parameter parameter δ is selected. Then the probability that the *j*-th parameter value δ is selected can be calculated by using (14).

$$\mathrm{AS}_j = \frac{\mathrm{Score}_j + 1}{\mathrm{num}_j + 1} \tag{13}$$

$$\mathrm{PLS}_j = \frac{\mathrm{AS}_j}{\sum \mathrm{AS}} \tag{14}$$

Step 5. Considering the fact that the information in the initial stage is less useful to the later stage, the PLS is initialized with 1/LS.size when the number of times that local search is performed is beyond a threshold. LS.size indicates how many there are parameter δ values, which is 4.

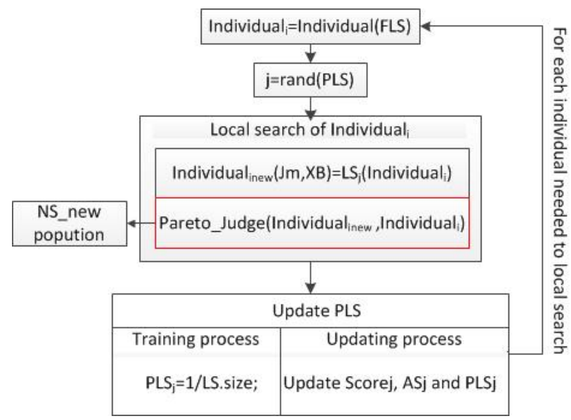

Fig. 7 Adaptive parameter determination in local search

IV. EXPERIMENT

A. *Parameter setting and comparison methods*

The proposed algorithm, ABOMC, is compared with several other clustering algorithms: the fuzzy c-means clustering algorithm (FCM), automatic fuzzy clustering using an improved differential evolution algorithm (FCIDE) [17] and NSDE-II. As should be noted that NSDE-II is to use differential evolution algorithm (DE) to substitute genetic algorithm in NSGA-II because of the powerful global search capability of DE.

In ABOMC, The probability for each individual to undergoing local search is 0.5. the maximum number of generation is 20. The size of population is 50.

B. *Experiment 1-FLC Multispectral Image*

In experiment 1, a Flightline C1 image of Tippecanoe County, Indiana, US, is used, which was acquired from the M7 scanner, at a resolution of 36.25 m × 36.25 m and a size of 97×102 pixels, in June 1966. Twelve bands are contained in this image. This image contains four classes: corn, oat, red clover, and wheat. The original image and the ground truth image are shown in Fig. 8 (a)–(b).

Fig. 8 (c)–(f) illustrates the clustering results of the FLC image using FCM, FCIDE, NSDE-II, and ABOMC, respectively. Visually, the clustering results of FCIDE, NSDE-II, and ABOMC are better than FCM due to the application of differential evolution algorithm. Because of the application of multi-objective optimization, NSDE-II, and ABOMC are better than FCIDE, especially for the corn class and red clover class. ABOMC achieves the best because there is less misclassification between corn class and red clover class.

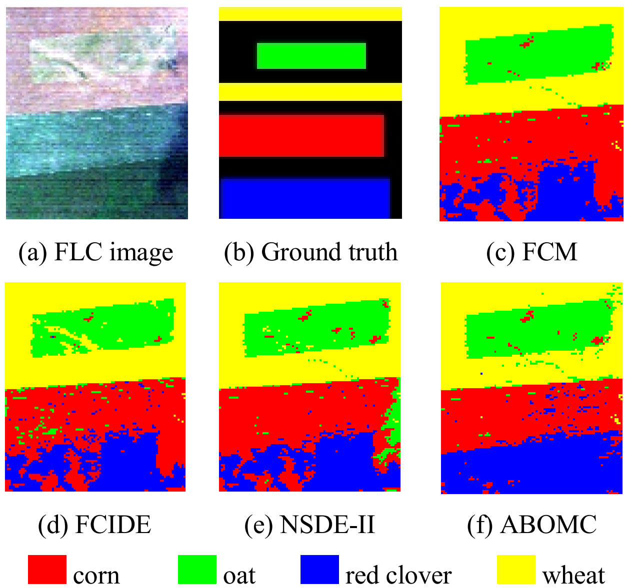

Fig. 8 FLC image and the classification results

Table I Comparison of the classification accuracy for the FLC image

Classes	FCM	FCIDE	NSDE-II	ABOMC
Producer's accuracy (%)				
Corn	97.90	92.90	97.88	93.86
Oat	96.90	88.50	94.69	97.48
Red clover	60.40	72.20	74.88	97.29
Wheat	99.50	100.0	99.52	97.28
User's accuracy (%)				
Corn	71.40	77.20	79.94	96.24
Oat	94.70	89.70	92.61	92.93
Red clover	99.40	96.00	98.84	94.68
Wheat	100.0	95.20	99.19	99.93
OA	87.09	87.98	90.96	96.35
Kappa	0.8228	0.8349	0.8759	0.9486

To compare the above algorithms quantitatively, the overall accuracy (OA) and kappa coefficient [18] for the image are listed in Table I. As can be seen from Table I, ABOMC obtains the best OA, 96.35%, with gains of 9.26%, 8.38%, and 5.39% over FCM, FCIDE, and NSDE-II, respectively. Overall, the quantitative comparison of the five algorithms is consistent with the above qualitative finding.

ABOMC achieves the best performance both visually and quantitatively. The reason for this may be that FCM can easily get stuck in a locally optimal solution, due to the lack of a global search capability. FCIDE is a single objective optimization method, which considers less information, compared with multi-objective optimization such as NSDE-II and ABOMC. Because of the application of the memetic algorithm with an adaptive parameter, ABOMC performs better.

C. *Experiment 2-Wuhan TM Image*

In order to further test the validity of the proposed algorithm, another image is used, which is a 30 m resolution multispectral Landsat TM image of Wuhan City, China, with a size of 400×400 pixels, and six bands. This region of the image was expected to contain five classes: river, vegetation, lake, bare soil, and building. The original Wuhan TM image and the ground truth image are shown in Fig. 9 (a)–(b).

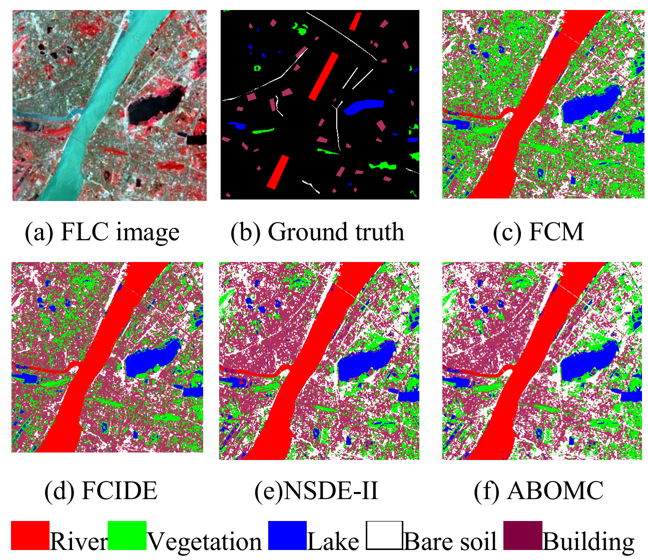

Fig. 9 WuhanTM image and the classification results

Fig. 9 (c)–(f) illustrates the clustering results of the FLC image using FCM, FCIDE, NSDE-II, and ABOMC, respectively. Firstly, as for the clustering result of FCM, there are many pixels that are misclassified into vegetation class, which is unreal. NSDE-II, and ABOMC perform better visual results, especially for the vegetation class in the right part of image. Furthermore, as for the vegetation class in the bottom right part of the image, ABOMC achieves a little better, compared with NSDE-II. On the whole, ABOMC achieves the best visual accuracy.

To compare the above algorithms quantitatively, the OA and kappa coefficient for the image are listed in Table II. ABOMC obtains the best OA, 91.29%, with gains of 9.63%, 5.6%, and 2.41% over FCM, FCIDE, and NSDE-II, respectively. The quantitative comparison of the four algorithms is consistent with the above qualitative finding:

based on the above analysis, ABOMC outperforms the three other classifiers.

Table II Comparison of the classification accuracy for the Wuhan TM image

Classes	FCM	FCIDE	NSDE-II	ABOMC
Producer's accuracy (%)				
River	100.00	100.00	100.00	100.00
Vegetation	82.50	89.18	86.04	93.68
Lake	99.80	100.00	99.55	99.87
Bare soil	71.80	67.93	81.51	85.35
Building	61.20	71.58	81.92	79.59
User's accuracy (%)				
River	100.0	100.00	100.00	100.00
Vegetation	75.10	82.20	96.97	98.23
Lake	91.90	96.34	90.02	95.46
Bare soil	85.10	84.41	73.13	67.65
Building	67.40	72.86	79.26	88.89
OA	81.66	85.69	88.88	91.29
Kappa	0.7619	0.8154	0.8574	0.8882

D. Analysis of parameter in Gaussian local search

One contribution of the paper is to adaptively determine the parameter in Gaussian local search, which controls the searching range and searching capability of local search. Fig. 10 lists the selection probability PLS of each local search with respect to the number of local search for Wuhan TM image. As has mentioned above, the PLS is initialized with 1/LS.size when the number that local search is performed is beyond a threshold. In this paper, the threshold is set as 80. As can be seen from Fig. 10, in different stages of the generation, different parameter values are selected for the local search, which is much suitable for the corresponding individual.

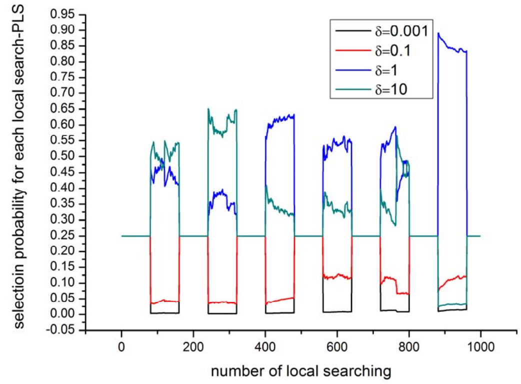

Fig. 10 The curve of PLS of each parameter value for Wuhan TM image

E. The Selection of Non-dominated Solutions from Pareto Front

As for ABOMC, Finally, many non-dominated individual will be generated in the pareto front. Here, we select the individual in the pareto front by trial and error to cluster the remote sensing image, i.e the individual with the best classification accuracy will be set as the clustering result. Fig. 11 lists the pareto fronts of ABOMC for Wuhan TM image. As for Wuhan TM image, the selected individual is in the middle part of the image.

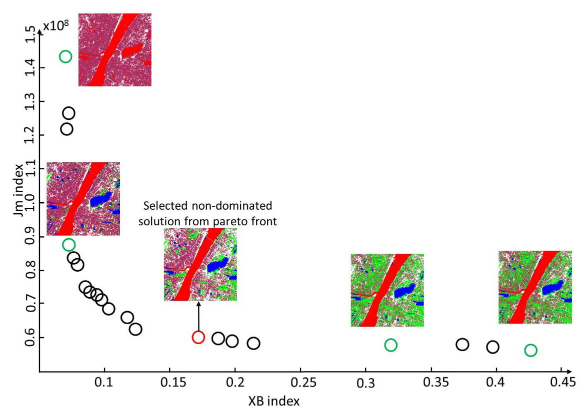

Fig. 11 The pareto front of Wuhan TM image

V. CONCLUSION

In this paper, an adaptive bi-objective memetic fuzzy clustering algorithm for remote sensing imagery (ABOMC) is proposed. In ABOMC, a bi-objective memetic framework is used to remote sensing image clustering. In addition, a parameter in local search can be determined adaptively by calculating the individual fitness increment before and after local search. A Pareto_Judge strategy is proposed to speed up the convergence and obtain more non-dominated individuals. Experiments are conducted to show the effectiveness of the proposed method. The proposed strategies make the information stored in the newly generated individuals fully utilized, resulting in more satisfactory remote sensing image clustering results.

However, one disadvantage of the proposed method is that it needs to select the non-dominated solution form the pareto front to cluster the remote sensing image manually, which is time-consuming. In our future work, more intelligent methods will be tested to select non-dominated solution from the pareto front. Also, spatial information is important in remote sensing image clustering. We will hybrid the spatial information the multi-objective memetic framework in the furture.

ACKNOWLEDGMENT

The authors would like to thank the editor, associate editor and anonymous reviewers for their helpful comments and suggestions.

REFERENCES

[1] A. Mukhopadhyay, U. Maulik, S. Bandyopadhyay, and C. Coello Coello, "A survey of multi-objective evolutionary algorithms for data mining: Part-II," IEEE Trans. Evol. Comput. , 2013.

[2] Y. Zhong, S. Zhang, and L. Zhang, "Automatic Fuzzy Clustering Based on Adaptive Multi-Objective Differential Evolution for Remote Sensing Imagery," IEEE Journal of Selected Topics in Applied Earth Observations and Remote Sensing 2013.

[3] A. Paoli, F. Melgani, and E. Pasolli, "Clustering of hyperspectral images based on multiobjective particle swarm optimization," IEEE Trans. Geosci. Remote Sens. , vol. 47, pp. 4175-4188, 2009.

[4] K. Deb, A. Pratap, S. Agarwal, and T. Meyarivan, "A fast and elitist multiobjective genetic algorithm: NSGA-II," IEEE Trans. Evol. Comput. , vol. 6, pp. 182-197, 2002.

[5] S. Das and P. N. Suganthan, "Differential evolution: A survey of the state-of-the-art," IEEE Trans. Evol. Comput. , vol. 15, pp. 4-31, 2011.

[6] Y. S. Ong, M. Lim, and X. Chen, "Memetic computation—Past, present & future," IEEE Comput. Intell. Mag. , vol. 5, pp. 24-31, 2010.

[7] U. Maulik and I. Saha, "Automatic Fuzzy Clustering Using Modified Differential Evolution for Image Classification," IEEE Trans. Geosci. Remote Sens. , vol. 48, pp. 3503-3510, 2010.

[8] A. Ghosh, A. Datta, and S. Ghosh, "Self-adaptive differential evolution for feature selection in hyperspectral image data," Applied Soft Computing, vol. 13, pp. 1969-1977, 2013.

[9] Y. Zhong, L. Zhao, and L. Zhang, "An adaptive sifferential evolution endmember extraction algorithm for hyperspectral remote sensing imagery," IEEE Geosci. Remote Sens. Lett. , DOI: 10.1109/LGRS.2013.2285476 2013.

[10] Y. Zhong and L. Zhang, "Sub-pixel Mapping Based on Artificial Immune Systems for Remote Sensing Imagery," Pattern Recognit. , vol. 46, pp. 2902-2926, 2013.

[11] W. Sheng, S. Swift, L. Zhang, and X. Liu, "A weighted sum validity function for clustering with a hybrid niching genetic algorithm," IEEE Trans. Syst. Man Cybern. Part B Cybern. , vol. 35, pp. 1156-1167, 2005.

[12] Q. Zhang and H. Li, "MOEA/D: A multiobjective evolutionary algorithm based on decomposition," IEEE Trans. Evol. Comput. , vol. 11, pp. 712-731, 2007.

[13] A. Zhou, B. Y. Qu, H. Li, S. Z. Zhao, P. N. Suganthan, and Q. Zhang, "Multiobjective evolutionary algorithms: A survey of the state of the art," Swarm and Evolutionary Computation, vol. 1, no. 1, pp. 32-49, 2011.

[14] X. Chen and Y.-S. Ong, "A conceptual modeling of meme complexes in stochastic search," IEEE Trans. Syst. Man Cybern. Part C Appl. Rev. , vol. 42, pp. 612-625, 2012.

[15] Y.-S. Ong, M.-H. Lim, N. Zhu, and K.-W. Wong, "Classification of adaptive memetic algorithms: a comparative study," IEEE Trans. Syst. Man Cybern. Part B Cybern. , vol. 36, pp. 141-152, 2006.

[16] J. Brest, S. Greiner, B. Boskovic, M. Mernik, and V. Zumer, "Self-adapting control parameters in differential evolution: A comparative study on numerical benchmark problems," IEEE Trans. Evol. Comput. , vol. 10, pp. 646-657, 2006.

[17] S. Das and A. Konar, “Automatic image pixel clustering with an improved differential evolution,” Appl. Soft Comput., vol. 9, no. 1, pp. 226–236, Jan. 2009.

[18] J. Cohen, "A coefficient of agreement for nominal scales," Educational and psychological measurement, vol. 20, pp. 37-46, 1960.